Catalysis Science & Technology

ROYAL SOCIETY OF CHEMISTRY

PAPER

View Article Online
View Journal | View Issue

Cite this: *Catal. Sci. Technol.*, 2023, 13, 6561

Efficient depolymerization of PET over Ti-doped SBA-15 with abundant Lewis acid sites *via* glycolysis†

Songlei Mo, Yong Guo, Xiaohui Liu and Yanqin Wang *

The glycolysis of polyethylene terephthalate (PET) is considered as the most promising PET recycling strategy due to its mild reaction conditions and circularity. Herein, several metal-doped SBA-15 (M/SBA-15) as heterogeneous Lewis acid catalysts were investigated to screen the best catalyst and to understand the essence for their differences in PET glycolysis. It is found that the catalytic activity is positively correlated with the acid amount in different metal-doped SBA-15 and Ti/SBA-15 with different Ti loadings, with the exception of Nb/SBA-15. 4Ti/SBA-15 with abundant Lewis acid sites shows excellent PET glycolysis ability, with the yield of bis(2-hydroxyethyl) terephthalate (BHET) reaching 87.2% within 45 min at 190 °C (isolated yield 73%). While 4Nb/SBA-15 has a similar acid amount as that in 4Ti/SBA-15, but it has very low catalytic activity probably due to its strong oxygen affinity. Acetone–methanol-adsorption DRIFTS confirms its strong oxygen affinity, which would poison the acid sites by ethylene glycol (EG) and result in very low activity. This study demonstrates that PET glycolysis activity is really correlated with the amount of Lewis acid sites, but species with very strong oxygen affinity would lower its activity. Further diffuse reflection ultraviolet-visible (DR UV-vis) spectra analysis confirms that tetrahedral Ti^{4+} species in Ti/SBA-15 is the real active center. In addition, 4Ti/SBA-15 has good reusability and can be used in common real PET (dyed polyester fabric, PET bottles) glycolysis. These results indicate that increasing the amount of Lewis acid sites is a promising way to enhance PET glycolysis and 4Ti/SBA-15 with high activity and stability is a potential catalyst for industrial application.

Received 14th August 2023,
Accepted 12th October 2023

DOI: 10.1039/d3cy01127e

rsc.li/catalysis

Introduction

PET is one of the most widely used synthetic polyester plastic, with nearly 70 million tons produced annually worldwide.[1] Due to the huge demand of PET and difficult degradation after use,[2,3] its recycling and upcycling have attracted increasing attention.[4,5] Chemical recycling is considered as the most promising strategy due to its sustainability and circularity,[4,6] and various methods have been developed, such as hydrolysis,[7–9] methanolysis,[10,11] glycolysis,[12–20] aminolysis,[21] and hydrogenolysis.[22–25] Among these methods, glycolysis is favored because it has the advantages of mild reaction conditions, easy separation of the target product (BHET), and direct use of BHET for repolymerization. It is mentioned that the product of PET hydrolysis (terephthalic acid) or methanolysis (dimethyl terephthalate) needs to undergo esterification or transesterification reaction to produce BHET before being repolymerized into PET.[4]

Currently, numerous heterogeneous catalysts for PET glycolysis, including heterogeneous basic catalysts (*e.g.*, Ca- and Mg-based catalysts)[18–20] and Lewis acid catalysts (*e.g.*, Zn-, Co-, Fe-, and Mn-based catalysts)[12–15] have been developed. Compared with homogeneous catalysts, heterogeneous catalysts are easy to separate from the product and have less influence on the purity of BHET. Scheme 1 shows the mechanisms of

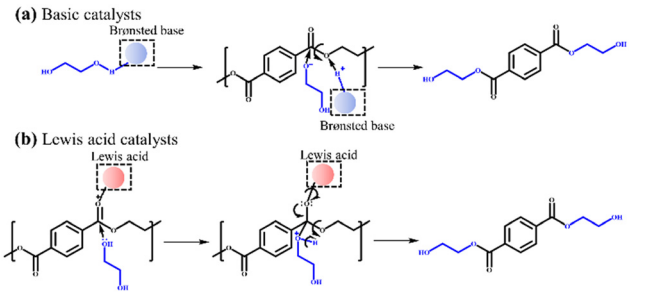

Scheme 1 Reaction mechanisms of PET glycolysis with (a) basic catalysts and (b) Lewis acid catalysts.

Shanghai Key Laboratory of Functional Materials Chemistry, Research Institute of Industrial Catalysis, School of Chemistry and Molecular Engineering, East China University of Science and Technology, Shanghai 200237, P. R. China.
E-mail: wangyanqin@ecust.edu.cn

† Electronic supplementary information (ESI) available. See DOI: https://doi.org/10.1039/d3cy01127e

depolymerizing PET catalyzed by basic catalysts and Lewis acid catalysts. The basic catalysts can activate EG through the deprotonation of the OH group by the Brønsted base sites to form catalytically active (and more nucleophilic) EG^- species.[6,13] Meanwhile, the Lewis acid catalysts can activate the C═O bonds in the PET chains *via* the Lewis acid sites to make the electrons of C═O bonds more biased toward oxygen.[13,14] The carbon atoms are then susceptible to being attacked by EG to achieve the transesterification reaction.

According to the literatures reported so far, the heterogeneous basic catalysts generally suffered from low reactivity and low yield of BHET (≤81%);[18–20] thus, heterogeneous Lewis acid catalysts have been extensively studied. Wu *et al.*[15] synthesized spinel-type MFe_2O_4 (M═Co, Ni, Cu, and Zn) to depolymerize PET *via* glycolysis and found that the glycolysis activity was positively correlated with Lewis acid strength. The stronger Lewis acid sites interacted more strongly with the C═O bonds in the PET chains, resulting in higher catalytic efficiency. Unfortunately, these catalysts were less active and took 6 h for total PET glycolysis, probably due to the less acid amounts of these metal composite oxides. Rinaldi and co-workers[14] prepared ultra-small cobalt nanoparticles modified with tannic acid, which made the catalyst highly dispersed in EG. The PET conversion and BHET isolated yield reached 96% and 77% at 180 °C within 3 h, respectively. Similarly, Wang *et al.*[12] synthesized Fe_3O_4 nano-dispersions modified with sodium citrate dihydrate for PET glycolysis. With this catalyst, PET can be completely depolymerized at 210 °C within 30 min, and the BHET yield reached 93%. All these works emphasized the importance of effective contact between the catalyst and PET, which seriously affected the depolymerization rate in PET glycolysis.

In addition to preparing ultra-small nanoparticles catalysts and modifying their surfaces to improve their dispersibility in EG, mesoporous catalysts with high specific surface area and rich pore structure would be another choice. The obvious advantage of this kind of catalyst is the easy separation compared to the nanoparticle catalyst. Therefore, in this work, the siliceous SBA-15, which has high specific surface area, rich pore structure, and is chemically inert, was selected as the catalyst support. In order to obtain an efficient PET glycolysis catalyst, we screened a series of representative metal ions (Nb,[26] Ti,[27] Zn,[28,29] Sn (ref. 30–32)) with Lewis acidity and doped them in SBA-15 to depolymerize PET. It is important to note here that after doping with different metal ions, the textural properties and acid strength of these catalysts are similar. A positive correlation between catalytic activity and acid amount was found in different metal-doped SBA-15 and Ti/SBA-15 with different Ti loadings. 4Ti/SBA-15 has rich Lewis acid sites and exhibits the most excellent glycolysis ability; the BHET yield reaches 87.2% within 45 min at 190 °C (isolated yield 73%). The exception is 4Nb/SBA-15, although it has relatively abundant acid sites, its ability to depolymerize PET is still poor. 4Ti/SBA-15 was further applied to depolymerize common real PET plastics, such as dyed polyester fabric, and PET bottles, and the yield of BHET is still maintained at about 85%. Importantly, this catalyst also has high stability, and the yield of BHET (~80%) does not decrease significantly during four cycles. In addition, in the scale-up experiment, the PET conversion is nearly 100% and the isolated BHET yield reaches 74%.

Experimental section

Materials

EG, acetonitrile, and $SnCl_4$ were purchased from Shanghai Macklin Biochemical Co., LTD. Tetrabutyl titanate and $Zn(NO_3)_2{\cdot}6H_2O$ were purchased from Aladdin Reagent Co., Ltd. Tetraethyl orthosilicate (TEOS) and HCl were purchased from Sinopharm Chemical Reagent Co., Ltd. Pluronic P123 triblock copolymer was purchased from Shanghai Sigma-Aldrich Co., Ltd. All chemicals were of analytical grade and used without further purification. PET was purchased from Aladdin Reagent Co., Ltd. PET bottles and dyed polyester fabric were purchased on commercial Taobao platform. The autoclave was purchased from Haian Petroleum Scientific Research Instrument Co., LTD, and the model was HKF-1.

Catalyst preparation

SBA-15 was synthesized according to previous reported procedures.[33] Typically, 2 g P123 was dissolved in 50 mL 1 mol L^{-1} HCl aqueous solution at 40 °C. After P123 was completely dissolved, 4.5 mL TEOS was added and continued to stir for 24 h at 40 °C. Until the stirring was over, the mixture was transferred into a Teflon-lined autoclave for crystallization at 100 °C for 2 days. The white solid products were obtained after vacuum filtration, washing with deionized water, drying at 60 °C, and calcination in turn. The calcination conditions: air atmosphere, 550 °C, heating rate 1 °C min^{-1}, 5 h.

Catalysts with different metal centers were prepared by the incipient wetness method. Firstly, SBA-15 was added to a certain concentration of metal precursor solution, and then *x*M/SBA-15 was obtained after drying and calcination in turn, where *x* represented the mass fraction of the corresponding metal M. The calcination conditions: air atmosphere, 500 °C, heating rate 3 °C min^{-1}, 4 h.

Characterization

The powder X-ray diffraction (XRD) patterns were recorded with a Rigaku D/max-2550VB/PC diffractometer using Cu Kα (λ = 0.15406 nm) radiation that was operated at 40 kV and 40 mA. The actual metal loading in the samples were detected by inductively coupled plasma-atomic emission spectroscopy (ICP-AES) on a PerkinElmer Optima 2100 DV spectrometer. Nitrogen adsorption–desorption isotherms of the catalysts were measured at −196 °C on a Micromeritics ASAP 2020 M sorption analyzer. Prior to the measurements, all the samples were pretreated at 120 °C for 8 h under vacuum. High-angle annular dark-field-scanning transmission electron microscopy (HADDF-STEM) images and energy dispersive spectrometer

(EDS) scanning of the samples were obtained on a Talos F200X TEM at 200 kV. ^{13}C nuclear magnetic resonance (NMR) spectra were recorded on an Ascend 600 MHz spectrometer, and DMSO-d_6 was used as the solvent. The differential scanning calorimetry (DSC) curve was obtained on a DSC 8500 calorimeter. The DR UV-vis spectra were recorded on a PerkinElmer Lambda 950 spectrometer.

NH_3-temperature-programmed desorption (NH_3-TPD) were carried out on a PX200 desorption apparatus. Typically, 50 mg catalyst was pretreated at 500 °C in Ar (50 mL min^{-1}) for 1 h and then cooled to 90 °C. The atmosphere was switched to 5% NH_3/Ar (50 mL min^{-1}), and the catalyst absorbed NH_3 for 40 min at 90 °C. After the adsorption was completed, the atmosphere was switched back to Ar (50 mL min^{-1}) and kept at 90 °C for 1 h to purge the residual NH_3 in the quartz tube. Finally, the temperature in the quartz tube increased from 90 °C to 500 °C at a heating rate of 10 °C min^{-1}, and the NH_3 signal was detected by a TCD detector.

Fourier Transform Infrared (FT-IR) spectra for pyridine adsorption were recorded on a Nicolet NEXUS 670 FT-IR spectrometer. All the catalysts were pretreated at 400 °C under vacuum for 1 h to remove physically adsorbed water and impurities on the catalyst surfaces. Next, the cell was cooled to 200 °C, and the FT-IR spectrum was recorded as the background. The temperature in the cell was continued to cool to room temperature, and pyridine vapor was then introduced into the cell at room temperature until equilibrium was reached. Subsequently, the temperature was increased to 200 °C and held for 30 min to achieve equilibrium between pyridine adsorption–desorption. After the equilibrium was reached, a second FT-IR spectrum was obtained. The spectra presented were obtained by subtracting the spectra recorded before and after pyridine adsorption.

The DRIFTS of acetone adsorption was recorded on a NICOLET iS50 FT-IR spectrometer equipped with an MCT/A detector. Firstly, the catalysts were pretreated *in situ* in the cell in Ar at 400 °C for 1 h, and the background spectra were recorded at 190 °C and 35 °C, respectively. Then, acetone with Ar was bubbled into the *in situ* cell for 40 min. Next, the cell was purged with Ar at 35 °C for 30 min, and the adsorption spectra of acetone were recorded. Finally, the temperature was increased to 190 °C, and the adsorption spectra were recorded. In addition, the DRIFTS of acetone adsorption involving the pretreatment of methanol were also recorded on the above instrument. The difference is that methanol needed to be bubbled into the *in situ* cell in advance before acetone.

General procedure for PET glycolysis

In a typical PET glycolysis reaction, PET (0.4 g), catalyst (50 mg), and EG (2.8 g) were loaded into a stainless-steel autoclave reactor (HKF-1). After N_2 purging three times, the reactor was charged to the target N_2 pressure (1 MPa), and the reaction was carried out at the target temperature (190 °C) at a magnetic stirring speed of 600 rpm. At the end of the reaction, the reactor was quenched to ambient temperature in an ice water bath. Acetonitrile was added to the reaction mixture to dissolve BHET and oligomers, and then the mixture was divided into two phases by centrifugation. The solid contained the catalyst and undepolymerized PET, and the liquid mainly contained the target product BHET and some oligomers. The solid was washed with ethanol, then dried, and weighed to quantify the undepolymerized PET mass. The quantitative analysis of BHET and oligomers (external standard method) was performed by an Agilent 1200 Series HPLC apparatus equipped with XDB-C18 (Eclipse USA) chromatographic column and G1314B ultraviolet detector (VWD). A mixture of water and methanol (volume ratio of 3 : 7) was used as the mobile phase with a flow of 0.45 mL min^{-1}, the ultraviolet (UV) wavelength was 254 nm, and the column temperature was maintained at 45 °C. The PET conversion and BHET yield can be obtained by the following equations, where m represents the mass, n represents the number of moles, and Mw_{PET} represents the molar masses of the PET repeating unit (192 g mol^{-1}).

$$\text{PET conversion} = \left(1 - \frac{m_{\text{undepolymerized PET}}}{m_{\text{initial PET}}}\right) \times 100\% \quad (1)$$

$$n_{\text{theoretical BHET}} = n_{\text{PET repeating units}} = \frac{m_{\text{initial PET}}}{Mw_{PET}} \quad (2)$$

$$\text{BHET yield} = \frac{n_{\text{produced BHET}}}{n_{\text{theoretical BHET}}} \times 100\% \quad (3)$$

The catalyst reusability experiment was carried out in the following steps. When the reaction was finished, acetonitrile was added to dissolve the BHET as well as the oligomers. The catalyst was then separated by centrifugation. The obtained catalyst was used directly in the next PET glycolysis reaction without calcination.

BHET was isolated by the method of József Kupai and co-workers.[16] Firstly, acetonitrile was removed from the reaction solution by distillation under reduced pressure, and then deionized water was added to the remaining solution. At this time, flocculation precipitates appeared in the solution, which was the BHET dimer. After BHET dimer was removed by filtration, the resulting filtrate was distilled to about 4 mL under reduced pressure. At last, the pure BHET crystal was obtained by storing the resulting solution in a refrigerator at 4 °C for 12 h. After filtration, washing, drying, and weighing, the isolated BHET yield can be calculated.

Results and discussion

Catalyst screening and the essence of catalysts affecting the performance

The glycolysis of PET was first carried out over various M/SBA-15 catalysts at 190 °C for 45 min, and the results are presented in Fig. 1a. The siliceous SBA-15 has poor catalytic activity, and the yield of BHET is only 0.9%. When the siliceous SBA-15 is doped with 4 wt% Ti or Zn, the yield of

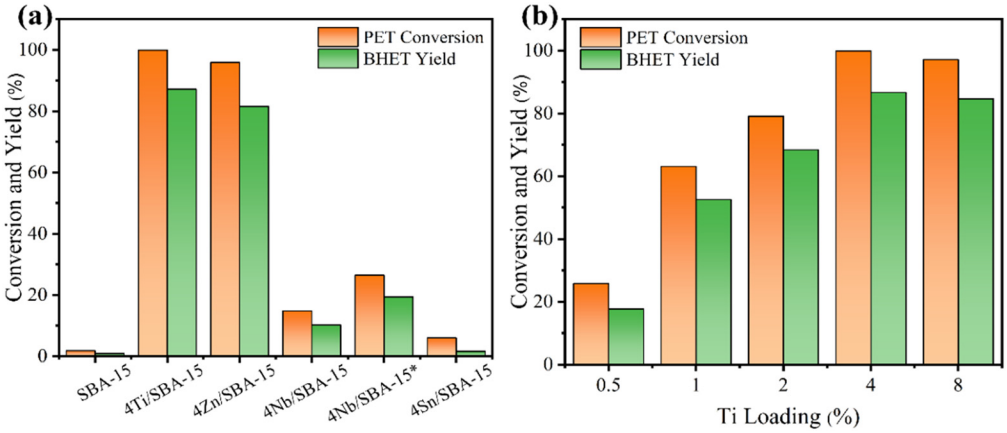

Fig. 1 (a) BHET yield obtained over different catalysts. Reaction conditions: 0.4 g PET, 2.8 g EG, 50 mg catalyst, 1 MPa N_2, 190 °C, 45 min. "*" means the reaction time is 2 h. (b) Influence of Ti loadings on BHET yield. Reaction conditions: 0.4 g PET, 2.8 g EG, 20 mg catalyst, 1 MPa N_2, 190 °C, 45 min.

BHET is significantly increased to 87.2% and 81.6%, respectively. Confusingly, 4Nb/SBA-15 and 4Sn/SBA-15, which also have acid sites, show poor glycolysis ability. Even on prolonging the reaction time to 2 h, the yield of BHET over 4Nb/SBA-15 was still low, only 19.4%. Due to the excellent catalytic activity of 4Ti/SBA-15, the influence of Ti loadings on PET glycolysis was further investigated. As shown in Fig. 1b, in the Ti loading range from 0.5 wt% to 4 wt%, the yield of BHET increased with Ti loading. However, on further increasing Ti loading to 8 wt%, the yield of BHET decreases slightly, which may be caused by the mass transfer limitation. The XRD patterns in Fig. S1d† show that high Ti loading leads to the aggregation of Ti species to form anatase, which decreases the specific surface area and blocks the pore of 8Ti/SBA-15 (Table S2†) and therefore affects the contact between PET and the active centers. All in all, 4Ti/SBA-15 shows the best PET glycolysis activity, and the yield of BHET reaches 87.2% in 45 min at 190 °C.

Next, we would like to find the differences of various M/SBA-15 catalysts and to correlate their properties with the catalytic performance. Obviously, here, the acid sites in these four investigated catalysts are the main catalytic active centers in PET glycolysis. Therefore, the NH_3-TPD was used to explore the acid properties in different metal-doped SBA-15 catalysts. As shown in Fig. 2a and Table S1,† the amount of acid sites of 4Sn/SBA-15 (0.04 mmol g^{-1}) is much less than that of the other three catalysts, which explains its lowest PET glycolysis activity. Meanwhile, 4Ti/SBA-15 and 4Zn/SBA-15 have abundant acid sites (0.24 mmol g^{-1}, 0.35 mmol g^{-1}, respectively) and thus show excellent glycolysis activity. In addition, it should be noted that although 4Zn/SBA-15 has the largest amount of acid sites, its catalytic activity is slightly lower than 4Ti/SBA-15, which may be caused by its lower specific surface area (Table S1†). The same rule appears in Ti/SBA-15 catalysts with different Ti loadings. With the increase in Ti loading, the amount of acid sites in Ti/SBA-15 catalysts increases and the BHET yield then gradually increases (Fig. 2b and Table S2†). An intriguing question is why 4Nb/SBA-15, which has similar acid amount to 4Ti/SBA-15 (0.22 mmol g^{-1}), exhibits poor PET glycolytic ability. Therefore, 4Ti/SBA-15 and 4Nb/SBA-15 were characterized in more detail to understand the reason for the difference in the catalytic activity between them.

Fig. 3a and b show the small- and wide-angle XRD patterns of 4Ti/SBA-15 and 4Nb/SBA-15. In the small-angle region, 4Ti/SBA-15 and 4Nb/SBA-15 have three distinct diffraction peaks at

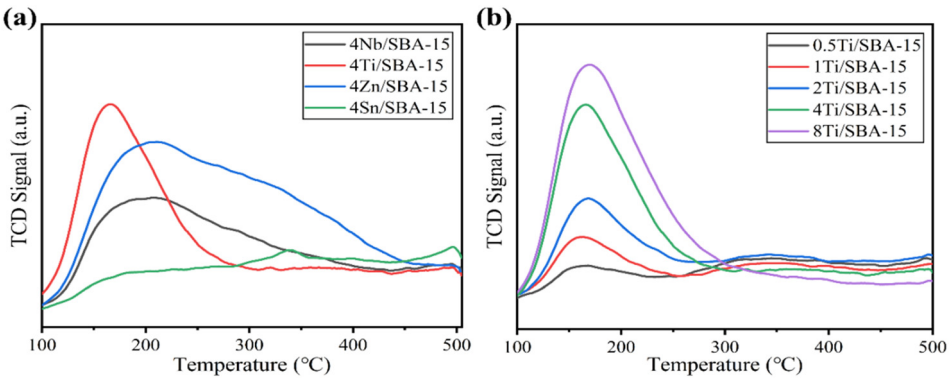

Fig. 2 (a) NH_3-TPD curves of various M/SBA-15 catalysts and (b) Ti/SBA-15 with different Ti loadings.

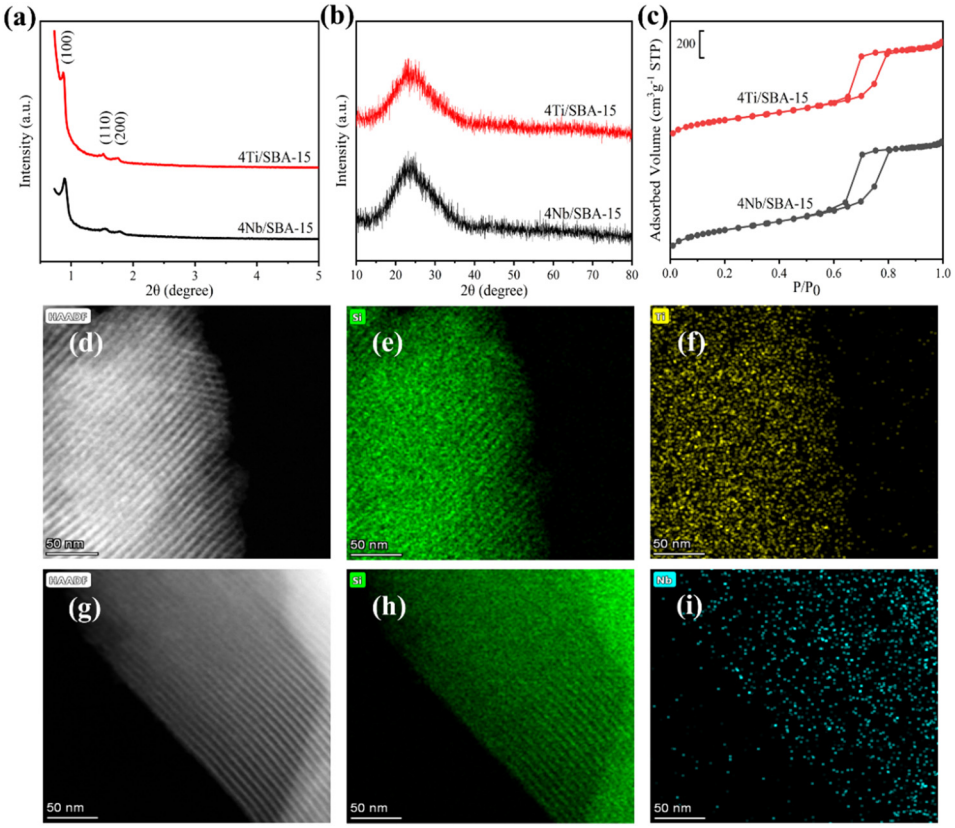

Fig. 3 (a) Small- and (b) wide-angle XRD patterns of 4Nb/SBA-15 and 4Ti/SBA-15. (c) N_2 adsorption-desorption isotherms of 4Nb/SBA-15 and 4Ti/SBA-15. (d) HADDF-STEM image of 4Ti/SBA-15. (e and f) EDS mapping images of Si (e) and Ti (f) in 4Ti/SBA-15. (g) HADDF-STEM image of 4Nb/SBA-15. (h and i) EDS mapping images of Si (h) and Nb (i) in 4Nb/SBA-15.

2θ = 0.8–2.0°, corresponding to the (100), (110), and (200) planes of the well-ordered *P6mm* structure in the sequence from left to right.[34] It indicates that the doping of Ti or Nb has little influence on pore ordering. In the wide-angle region, 4Ti/SBA-15 or 4Nb/SBA-15 has a characteristic band at 2θ = 15–35°, attributed to the amorphous silica framework. Fig. 3c shows the N_2 adsorption–desorption isotherms of 4Ti/SBA-15 and 4Nb/SBA-15. The isotherms of both samples are type IV possessing a H1 hysteresis loop, indicating that both samples are mesoporous materials with well-ordered, regular, cylindrical pores. In addition, the specific surface areas of 4Ti/SBA-15 and 4Nb/SBA-15 are 835 $m^2\ g^{-1}$ and 957 $m^2\ g^{-1}$, respectively (Table S1†). HAADF-STEM images (Fig. 3d and g) show that the long-range ordered structure and mesoporous structure of SBA-15 are maintained when Ti or Nb species is doped, which further confirms the characterization results of XRD and N_2 adsorption–desorption. The EDS mappings (Fig. 3f and i) reveal that Ti or Nb species is uniformly distributed on the siliceous SBA-15. The acid types of 4Ti/SBA-15 and 4Nb/SBA-15 were further investigated by FT-IR of pyridine adsorption. As shown in Fig. 4, the sharp 1450 cm^{-1} band is seen for both catalysts; meanwhile, no signal is observed at 1540 cm^{-1}. It is evident that the 4Ti/SBA-15 and 4Nb/SBA-15 catalysts have a majority of Lewis acid sites, in line with the results reported in the literature.[26,27]

The above characterizations show that 4Ti/SBA-15 and 4Nb/SBA-15 have very similar textural properties and acidic properties. Hence, it is puzzling why 4Nb/SBA-15 acts poorly in PET glycolysis. It is accepted that the activation of C═O bonds in PET chains is the key step in the reaction of PET glycolysis catalyzed by Lewis acid catalysts. But, on the other hand, if EG, another reactant and also a solvent, is adsorbed

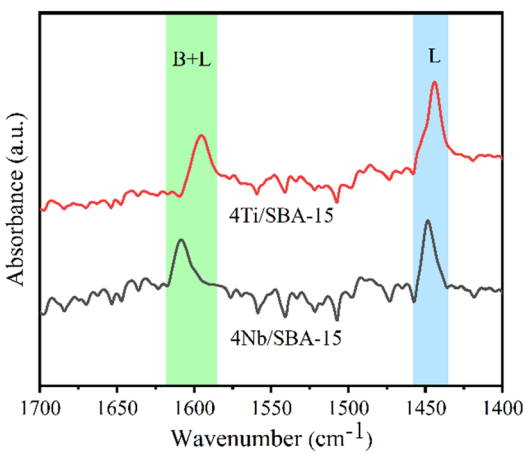

Fig. 4 FT-IR spectra of pyridine adsorbed on 4Nb/SBA-15 and 4Ti/SBA-15 recorded at 200 °C.

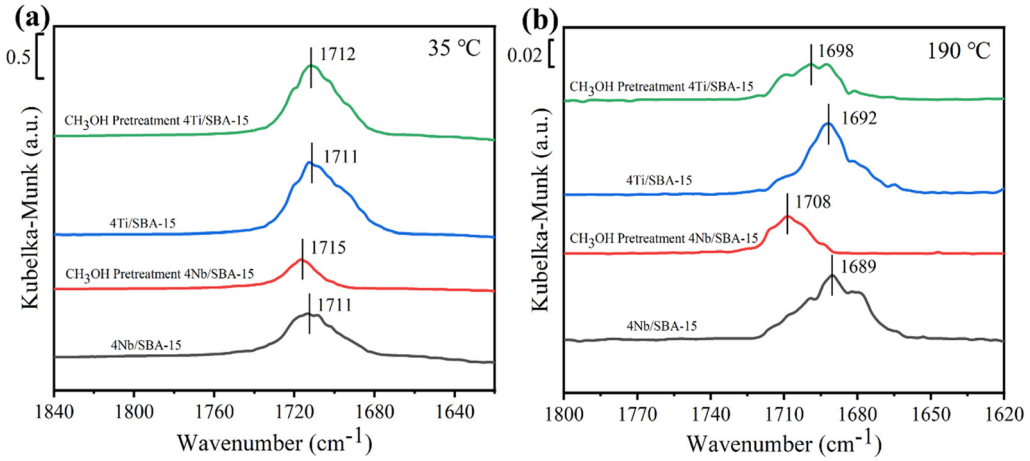

Fig. 5 Acetone DRIFTS spectra of 4Nb/SBA-15, 4Nb/SBA-15 pretreated with methanol, 4Ti/SBA-15, and 4Ti/SBA-15 pretreated with methanol recorded at (a) 35 °C and (b) 190 °C, respectively.

too strong on the catalyst surface, it would poison the Lewis acid sites, which was found in a methanol-poisoned system before.[35] Therefore, we further verified the effect of alcohols on the adsorption–activation of C=O bond over two catalysts. Acetone as a simple C=O bond-containing molecule was used to perform adsorption–desorption DRIFTS experiments on 4Ti/SBA-15, 4Ti/SBA-15-methanol (pre-adsorption of methanol for 40 min), and 4Nb/SBA-15, 4Nb/SBA-15-methanol. For gas-phase acetone, the stretching vibration peak of the C=O bond is at 1730 cm^{-1} band.[35,36] A significant red shift is observed for both 4Ti/SBA-15 and 4Nb/SBA-15, which is located at 1710 cm^{-1} and 1712 cm^{-1}, respectively. When these two catalysts are pretreated with methanol, the C=O bond signal on 4Ti/SBA-15 hardly changes, while the peak area of the C=O bond signal on 4Nb/SBA-15 decreases obviously, despite the red shift being preserved, suggesting that part of the active sites are poisoned by methanol. When the temperature increases to 190 °C (reaction temperature), the stretching vibration peaks of the C=O bond on these two catalysts are both blue shifted after methanol pretreatment, and the blue shift is more intense on 4Nb/SBA-15 (Fig. 5b). It indicates that the active sites of 4Ti/SBA-15 exhibit weak adsorption of methanol and therefore have little effect on the subsequent activation of the acetone C=O bond. For 4Nb/SBA-15, the strong oxygen affinity leads to the strong adsorption of methanol, which poisons the active sites[35] and leads to weak C=O bond activation. In view of this, we reasonably believe that 4Ti/SBA-15, which is dominated by Lewis acid sites, can activate C=O bonds in PET chains under the reaction conditions, and PET can be effectively depolymerized. However, 4Nb/SBA-15 will be poisoned by EG due to its strong oxygen affinity, resulting in the inactivation of C=O bonds in the PET chains. Thus, PET glycolysis cannot be carried out efficiently.

Optimization of PET glycolysis conditions

The influence of reaction temperature, time, and catalyst dosage on PET conversion and products yield were investigated. Fig. 6a shows the effect of reaction temperature on PET glycolysis, and it is found that the reaction temperature greatly affects the conversion of PET and the

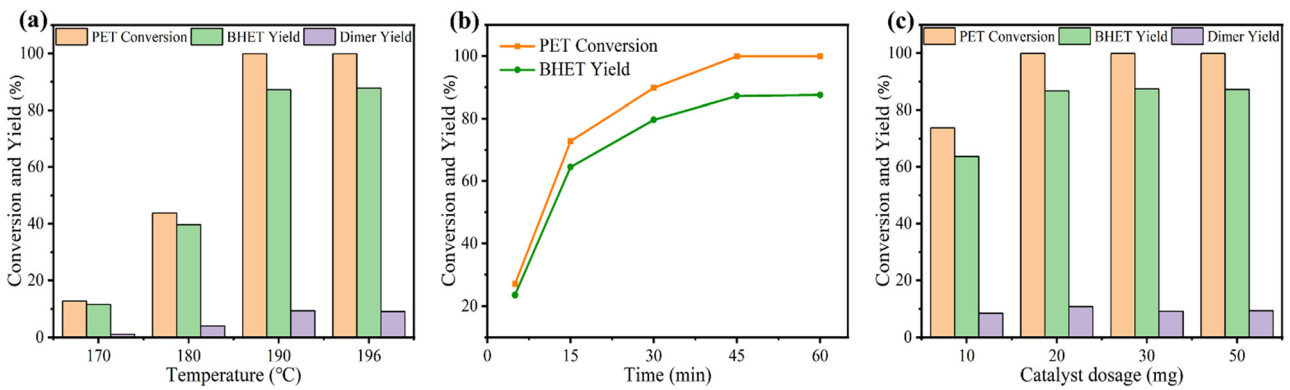

Fig. 6 (a) Influence of reaction temperature on PET conversion and BHET yield. Reaction conditions: 0.4 g PET, 2.8 g EG, 50 mg 4Ti/SBA-15, 1 MPa N_2, 45 min. (b) Reaction time curves of PET glycolysis. Reaction conditions: 0.4 g PET, 2.8 g EG, 50 mg 4Ti/SBA-15, 1 MPa N_2, 190 °C. (c) Influence of catalyst dosage on PET conversion and BHET yield. Reaction conditions: 0.4 g PET, 2.8 g EG, 1 MPa N_2, 190 °C, 45 min.

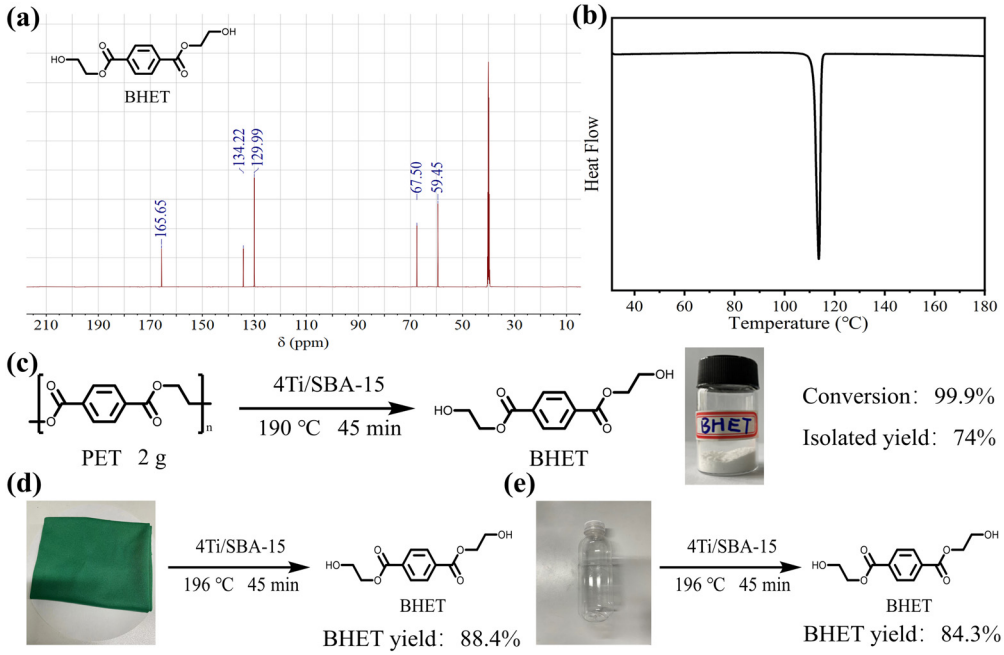

Fig. 7 (a) ^{13}C NMR spectrum and (b) DSC curve of BHET obtained from PET glycolysis. (c) The flow chart of PET glycolysis scale-up experiment. (d and e) The flow charts of common real PET plastics glycolysis.

yield of BHET. As the reaction temperature increases from 170 °C to 190 °C, the conversion of PET and the yield of BHET increase from 12.8% to 99.9% and 11.6% to 87.2%, respectively. This is because PET glycolysis is an endothermic reaction, and increasing the temperature is conducive to the reaction. The reaction time curve is present in Fig. 6b and shows that the conversion of PET and the yield of BHET gradually increase with the extension of the reaction time. After 45 min, the reaction reaches equilibrium and the yield of BHET is no longer increased. Next, we explored the influence of catalyst dosage on PET glycolysis (Fig. 6c). When the dosage of catalyst is reduced from 50 mg to 20 mg, the PET conversion and BHET yield are still maintained at a high level of 99.9% and 86.7%, respectively, indicating its high activity. But when it is further reduced to 10 mg, the PET conversion and BHET yield significantly decrease to 73.8% and 63.7%, respectively. The best reaction conditions are 190 °C, 45 min, PET/catalyst ratio = 0.4 g/20 mg = 20. We further compared 4Ti/SBA-15 with some recently reported catalysts for PET glycolysis. As shown in Table S5,† considering the reaction temperature, reaction time, and BHET yield, the catalytic performance of 4Ti/SBA-15 for PET glycolysis is at the forefront of these reported catalysts.

Under the optimal conditions of PET glycolysis, the pure BHET crystal is obtained by special separation methods,[16] and the isolated yield reaches 73%. The purity of the thus-obtained BHET crystal was further verify by ^{13}C NMR spectroscopy and DSC (Fig. 7). The signals at 59.45, 67.50, 129.99, 134.22, and 166.65 ppm in Fig. 7a are attributable to the BHET monomer reported in the literature.[14,37] The signal at about 40 ppm is attributable to the solvent, DMSO-d_6. Furthermore, the signal at about 63.0 ppm corresponding to the BHET dimer is not observed in this spectrum. The DSC curve in Fig. 7b shows that only an endothermic peak corresponding to the melting point of BHET crystals is observed at 113 °C, while the melting point peak of the BHET dimer is not observed at 170 °C,[38] further confirming the results of the ^{13}C NMP spectrum, *i.e.*, the BHET is pure after separation. Moreover, when maintaining the same ratio of catalyst and EG to PET but increasing the amount of PET to five times, the PET can still be fully depolymerized, with the BHET yield reaching 86.3% (isolated yield 74%, Fig. 7c). Finally, the 4Ti/SBA-15 catalyst was used for common real PET plastics, such as dyed polyester fabric and PET bottles, and it was found that the yield of BHET still reached about 85% (Fig. 7d and e). It is important to note that the pigments

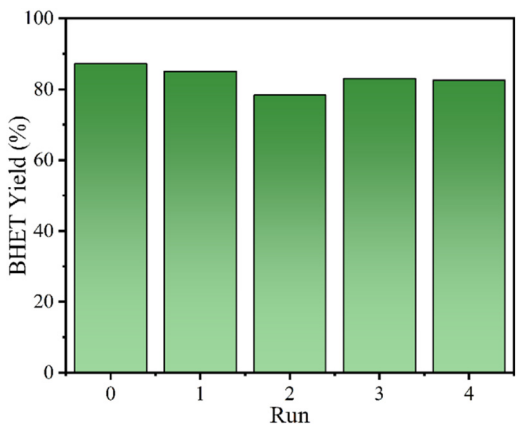

Fig. 8 The reusability of 4Ti/SBA-15 in the glycolysis of PET. Reaction conditions: 0.4 g PET, 2.8 g EG, 30 mg 4Ti/SBA-15, 1 MPa N_2, 196 °C, 45 min.

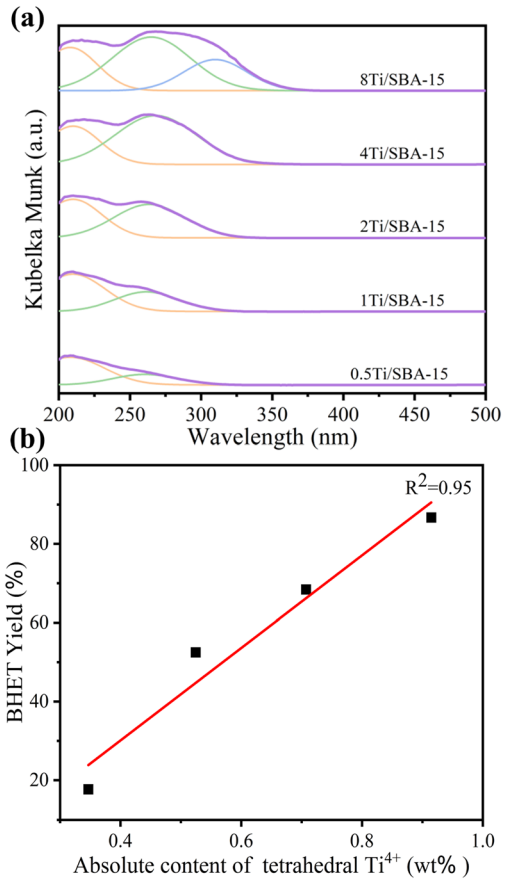

Fig. 9 (a) DR UV-vis spectra of Ti/SBA-15 with different Ti loadings. (b) The linear relationship between the absolute content of tetrahedral Ti^{4+} species and the BHET yield.

in dyed polyester fabric do not affect the PET glycolysis process but will affect the purity of the obtained BHET (pigments will residue in BHET, Fig. S3†).

Fig. 8 shows the reusability of 4Ti/SBA-15 in the glycolysis of PET. In four cycles, 4Ti/SBA-15 can efficiently catalyze PET glycolysis, and the yield of BHET is maintained at about 80%. The slight decrease in BHET yield may be due to the inevitable physical losses during the recovery of the catalyst. Inspiringly, 4Ti/SBA-15 still shows excellent catalytic activity and stability in a mixed plastic (PE + PS + PET, Fig. S4†). Fig. S5† shows the small-angle and wide-angle XRD patterns of 4Ti/SBA-15 after the reaction. In the small-angle and wide-angle range, the diffraction peak of 4Ti/SBA-15 is almost unchanged compared with the fresh catalyst, indicating that it has stable structural properties.

The real active sites in Ti/SBA-15 and proposed reaction mechanism

To further identify the active site in the process of PET glycolysis catalyzed by Ti/SBA-15, the DR UV-vis spectra were used to investigate the chemical environment of Ti species in Ti/SBA-15 catalysts. As shown in Fig. 9a, in the Ti loading range from 0.5 wt% to 4 wt%, the ligand to metal charge transfer (LMCT) bands from O^{2-} to Ti^{4+} in the tetrahedral and octahedral coordination spheres were observed at about 215 nm and 260 nm, respectively.[27,39] Further increasing the Ti loading to 8 wt%, there was a new band centered at about 310 nm, suggesting the emergence of polymerized Ti species,[27] which is consistent with the XRD results (the appearance of anatase phase, Fig. S1d†). Combined with the ICP results, the absolute contents of tetrahedral Ti^{4+} species in Ti/SBA-15 catalysts with different Ti loadings were calculated by multiplying the actual Ti loading by the relative content of tetrahedral Ti^{4+} species (based on the percentage of peak area) and fitted to the correlation with the BHET yield. Interestingly, the linear correlation coefficient R^2 between the absolute content of tetrahedral Ti^{4+} species and the BHET yield is 0.95, suggesting that the tetrahedral Ti^{4+} species as the Lewis acid site[27] is the main active center for depolymerizing PET (Fig. 9b).

The reaction process of PET glycolysis is proposed as follows (Scheme 2). First, the C═O bond in the PET chain is activated by the tetrahedral Ti^{4+} species, causing the electrons in the C═O bond to deviate toward the oxygen atom. And then, the carbon atom is vulnerable to attack by the free lone pairs of electrons on the oxygen of EG. Finally, the C–O bond in the PET chain is broken and a new C–O bond with EG is formed. Repeating in this way, the polymer PET was eventually depolymerized into BHET monomer.

Conclusions

In summary, we screened a series of heterogeneous Lewis acid catalysts to depolymerize PET and found that the

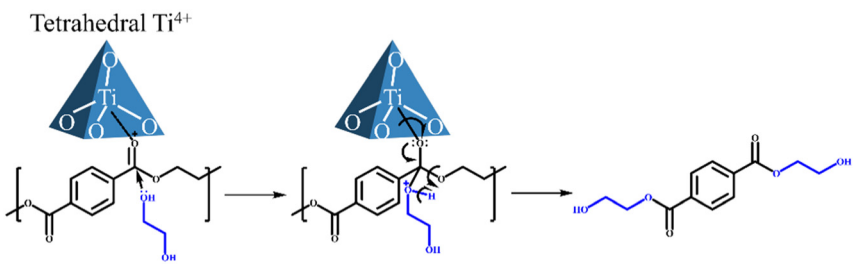

Scheme 2 Reaction mechanism of PET glycolysis catalyzed by Ti/SBA-15.

amount of acid sites and the oxygen affinity of the catalysts severely affect PET glycolysis. Among the four investigated M/SBA-15 catalysts, 4Ti/SBA-15 with abundant Lewis acid sites shows the best PET glycolysis activity, and the BHET yield reaches 87.2% (isolated yield 73%) at 190 °C for 45 min. The DR UV-vis spectra confirm that the tetrahedral Ti^{4+} species is the main active center. Importantly, the catalyst also has high stability, and the yield of BHET does not decrease during four cycles. In addition, 4Ti/SBA-15 can be used to depolymerize common real PET plastics, such as dyed polyester fabric and PET bottles. Inspiringly, the catalyst still maintains high activity, and the dyes in the fabric have little effect on the glycolysis process. The above results show that the catalyst has the prospect of industrial application.

Conflicts of interest

There are no conflicts to declare.

Acknowledgements

This work was supported financially by the NSFC of China (22102056, 21832002), China.

Notes and references

1 Z. W. Gao, B. Ma, S. Chen, J. Q. Tian and C. Zhao, *Nat. Commun.*, 2022, **13**, 3343.
2 W. Cornwall, *Science*, 2021, **373**, 37–39.
3 E. Meyer-Cifuentes, J. Werner, N. Jehmlich, S. E. Will, M. Neumann-Schaal and B. Ozturk, *Nat. Commun.*, 2020, **11**, 5790.
4 E. Barnard, J. J. R. Arias and W. Thielemans, *Green Chem.*, 2021, **23**, 3765–3789.
5 Q. D. Hou, M. N. Zhen, H. L. Qian, Y. F. Nie, X. Y. Bai, T. L. Xia, M. L. U. Rehman, Q. S. Li and M. T. Ju, *Cell Rep. Phys. Sci.*, 2021, **2**, 100514.
6 M. Y. Chu, Y. Liu, X. X. Lou, Q. Zhang and J. X. Chen, *ACS Catal.*, 2022, **12**, 4659–4679.
7 M. J. Kang, H. J. Yu, J. Jegal, H. S. Kim and H. G. Cha, *Chem. Eng. J.*, 2020, **398**, 125655.
8 S. Ugduler, K. M. Van Geem, R. Denolf, M. Roosen, N. Mys, K. Ragaert and S. De Meester, *Green Chem.*, 2020, **22**, 5376–5394.
9 Y. Q. Wang, Y. Zhang, H. Y. Song, Y. X. Wang, T. S. Deng and X. L. Hou, *J. Cleaner Prod.*, 2019, **208**, 1469–1475.
10 M. Genta, T. Iwaya, M. Sasaki, M. Goto and T. Hirose, *Ind. Eng. Chem. Res.*, 2005, **44**, 3894–3900.
11 Z. T. Laldinpuii, V. Khiangte, S. Lalhmangaihzuala, C. Lalmuanpuia, Z. Pachuau, C. Lalhriatpuia and K. Vanlaldinpuia, *J. Polym. Environ.*, 2022, **30**, 1600–1614.
12 Q. Sun, Y. Y. Zheng, L. X. Yun, H. Wu, R. K. Liu, J. T. Du, Y. H. Gu, Z. G. Shen and J. X. Wang, *ACS Sustainable Chem. Eng.*, 2023, **11**, 7586–7595.
13 H. Zhang, J. I. Choi, J. W. Choi, S. M. Jeong, P. S. Lee and D. Y. Hong, *J. Ind. Eng. Chem.*, 2022, **115**, 251–262.
14 F. R. Veregue, C. T. P. da Silva, M. P. Moises, J. G. Meneguin, M. R. Guilherme, P. A. Arroyo, S. L. Favaro, E. Radovanovic, E. M. Girotto and A. W. Rinaldi, *ACS Sustainable Chem. Eng.*, 2018, **6**, 12017–12024.
15 P. A. Krisbiantoro, Y. W. Chiao, W. S. Liao, J. P. Sun, D. Tsutsumi, H. Yamamoto, Y. Kamiya and K. C. W. Wu, *Chem. Eng. J.*, 2022, **450**, 137926.
16 Z. Feher, J. Kiss, P. Kisszekelyi, J. Molnar, P. Huszthy, L. Karpati and J. Kupai, *Green Chem.*, 2022, **24**, 8447–8459.
17 N. H. Le, T. T. N. Van, B. Shong and J. Cho, *ACS Sustainable Chem. Eng.*, 2022, **10**, 17261–17273.
18 Y. J. Zhao, M. S. Liu, R. Y. Zhao, F. S. Liu, X. P. Ge and S. T. Yu, *Res. Chem. Intermed.*, 2018, **44**, 7711–7729.
19 F. F. Chen, G. H. Wang, W. Li and F. Yang, *Ind. Eng. Chem. Res.*, 2013, **52**, 565–571.
20 I. Yunita, S. Putisompon, P. Chumkaeo, T. Poonsawat and E. Somsook, *Chem. Pap.*, 2019, **73**, 1547–1560.
21 A. Jain and R. K. Soni, *J. Polym. Res.*, 2007, **14**, 475–481.
22 S. L. Lu, Y. X. Jing, B. Feng, Y. Guo, X. H. Liu and Y. Q. Wang, *ChemSusChem*, 2021, **14**, 4242–4250.
23 Y. X. Jing, Y. Q. Wang, S. Y. Furukawa, J. Xia, C. Y. Sun, M. J. Hulsey, H. F. Wang, Y. Guo, X. H. Liu and N. Yan, *Angew. Chem., Int. Ed.*, 2021, **60**, 5527–5535.
24 S. Westhues, J. Idel and J. Klankermayer, *Sci. Adv.*, 2018, **4**, eaat9669.
25 Y. Kratish and T. J. Marks, *Angew. Chem., Int. Ed.*, 2022, **61**, e202112576.
26 F. Xue, D. Ma, T. Tong, X. H. Liu, Y. F. Hu, Y. Guo and Y. Q. Wang, *ACS Sustainable Chem. Eng.*, 2018, **6**, 13107–13113.
27 S. Y. Chen, T. Mochizuki, Y. Abe, M. Toba and Y. Yoshimura, *Appl. Catal., B*, 2014, **148**, 344–356.
28 J. M. Du, H. L. Xu, J. Shen, J. J. Huang, W. Shen and D. Y. Zhao, *Appl. Catal., A*, 2005, **296**, 186–193.
29 L. Lin, J. X. Liu, X. T. Zhang, J. L. Wang, C. Y. Liu, G. Xiong and H. C. Guo, *Ind. Eng. Chem. Res.*, 2020, **59**, 16146–16160.
30 M. Asakawa, A. Shrotri, H. Kobayashi and A. Fukuoka, *Green Chem.*, 2019, **21**, 6146–6153.
31 I. Aguas, M. J. Hidalgo, A. L. Villa and E. A. Alarcon, *Catal. Today*, 2022, **394**, 403–413.
32 W. L. Dai, Q. F. Lei, G. J. Wu, N. J. Guan, M. Hunger and L. D. Li, *ACS Catal.*, 2020, **10**, 14135–14146.
33 T. L. Jiang, H. X. Tao, J. W. Ren, X. H. Liu, Y. Q. Wang and G. Z. Lu, *Microporous Mesoporous Mater.*, 2011, **142**, 341–346.
34 D. Y. Zhao, J. L. Feng, Q. S. Huo, N. Melosh, G. H. Fredrickson, B. F. Chmelka and G. D. Stucky, *Science*, 1998, **279**, 548–552.
35 Y. X. Jing, M. Shakouri, X. H. Liu, Y. F. Hu, Y. Guo and Y. Q. Wang, *ACS Catal.*, 2022, **12**, 10690–10699.
36 J. Q. Wang, X. Wang, Z. T. Cui, B. Liua and M. H. Cao, *Phys. Chem. Chem. Phys.*, 2015, **17**, 14185–14192.
37 L. Bartolome, M. Imran, K. G. Lee, A. Sangalang, J. K. Ahn and D. H. Kim, *Green Chem.*, 2014, **16**, 279–286.
38 G. X. Xi, M. X. Lu and C. Sun, *Polym. Degrad. Stab.*, 2005, **87**, 117–120.
39 P. Wu, T. Tatsumi, T. Komatsu and T. Yashima, *J. Catal.*, 2001, **202**, 245–255.